Chinese Physics Letters 41, 117401 (2024) Express Letter

Observation of Zero-Energy Modes with Possible Time-Reversal Symmetry Breaking on Step Edge of $CaKFe_4As_4$

Lu Cao(曹路)[1,2†], Geng Li(李更)[1,2,3†], Wenyao Liu(刘文尧)[1,2,3†], Ya-Bin Liu(刘亚彬)[4], Hui Chen(陈辉)[1,2], Yuqing Xing(邢宇庆)[1,2], Lingyuan Kong(孔令元)[1,2], Fazhi Yang(杨发枝)[1,2,3], Quanxin Hu(胡全欣)[1,2,3], Meng Li(李萌)[1,2], Xingtai Zhou(周兴泰)[1,2], Zichao Chen(陈子超)[1,2], Chenhang Ke(柯晨航)[5], Lunhui Hu(胡仑辉)[4], Guang-Han Cao(曹光旱)[4], Congjun Wu(吴从军)[5,6,7,8], Hong Ding(丁洪)[9,1,3*], and Hong-Jun Gao(高鸿钧)[1,2,3*]

[1]*Institute of Physics, Chinese Academy of Sciences, Beijing 100190, China*
[2]*School of Physical Sciences, University of Chinese Academy of Sciences, Beijing 100049, China*
[3]*Hefei National Laboratory, Hefei 230088, China*
[4]*Department of Physics, Zhejiang University, Hangzhou 310027, China*
[5]*New Cornerstone Science Laboratory, Department of Physics, School of Science, Westlake University, Hangzhou 310024, China*
[6]*Institute for Theoretical Sciences, Westlake University, Hangzhou 310024, China*
[7]*Key Laboratory for Quantum Materials of Zhejiang Province, School of Science, Westlake University, Hangzhou 310024, China*
[8]*Institute of Natural Sciences, Westlake Institute for Advanced Study, Hangzhou 310024, China*
[9]*Tsung-Dao Lee Institute, and New Cornerstone Science Laboratory, Shanghai Jiao Tong University, Shanghai 201210, China*

(Received 28 August 2024; accepted manuscript online 30 September 2024)

Topologically nontrivial Fe-based superconductors attract extensive attentions due to their ability of hosting Majorana zero modes (MZMs) which could be used for topological quantum computation. Topological defects such as vortex lines are required to generate MZMs. Here, we observe the robust edge states along the surface steps of $CaKFe_4As_4$. Remarkably, the tunneling spectra show a sharp zero-bias peak (ZBP) with multiple integer-quantized states at the step edge under zero magnetic field. We propose that the increasing hole doping around step edges may drive the local superconductivity into a state with possible spontaneous time-reversal symmetry breaking. Consequently, the ZBP can be interpreted as an MZM in an effective vortex in the superconducting topological surface state by proximity to the center of a tri-junction with different superconducting order parameters. Our results provide new insights into the interplay between topology and unconventional superconductivity, and pave a new path to generate MZMs without magnetic field.

DOI: 10.1088/0256-307X/41/11/117401

Fe-based superconductors (FeSCs) exhibit a wide range of fascinating phenomena attributable to their multiband superconducting nature.[1–4] Recently, the superconducting topological surface states have been discovered in several FeSCs such as Fe(Te,Se),[5] ($Li_{0.84}Fe_{0.16}$)OHFeSe,[6] $CaKFe_4As_4$,[7] and LiFeAs.[8–12] These superconducting topological surface states share similar properties to chiral $p+ip$ superconductors.[13] The Majorana zero modes (MZMs) in magnetic vortex cores[6,7,9,11,12,14–17] and possible chiral Majorana states at the domain walls[18] have been observed in many FeSCs samples. However, unlike the chiral $p+ip$ superconductors, the superconducting topological surface states do not have a well-defined edge, which results in the lacking of Majorana modes on the edges for these FeSCs. In this Letter, we report a surprising observation of a robust edge state with zero modes without magnetic field on the step edges of $CaKFe_4As_4$ with scanning tunneling microscopy/spectroscopy (STM/S).

The crystal structure of $CaKFe_4As_4$ is similar to the 122-type Fe–As superconductors such as $BaFe_2As_2$ but with Ca and K layers alternately inserting between Fe–As layers[19] [Fig. 1(a)]. Recently, the superconducting topological surface state has been observed in $CaKFe_4As_4$.[7] As in Fe(Te,Se), where evidence of Majorana modes has been spotted on the domain walls[18] and line defects,[20] we are motivated to search for possible Majorana modes around the defect sites such as step edge and domain boundary in this topologically non-trivial FeSC material.

After cleavage, some steps naturally form on the surface of a high-quality $CaKFe_4As_4$ single crystal[21] [Fig. 1(b)]. In the region shown in Fig. 1(c), a sharp and

†These authors contributed equally to this work.
*Corresponding authors. Email: hjgao@iphy.ac.cn; dingh@sjtu.edu.cn

straight step with a height of 1.3 nm is observed, consistent with one unit cell (1 u.c.) of the $CaKFe_4As_4$ crystal along the ***c*** axis. The zero-energy differential conductance (ZEDC) map clearly displays a pronounced density of states (DOS) along the step edge [Fig. 1(d)], indicating the existence of a robust edge state. Its intensity decays slowly across a range of ~ 10 nm into the upper terrace [Fig. 1(e)], whereas it drops abruptly to zero on the lower terrace side [also see the orange curve in Fig. 2(e)]. In addition, we find that the edge state is ubiquitous and continuous at the kinks or corners of a step [Fig. 1(f)], indicating that the observed edge state is robust and independent of the orientations of step edges. The differential conductance maps of the edge states at other energies are shown in Fig. S1 in the Supplementary Material.

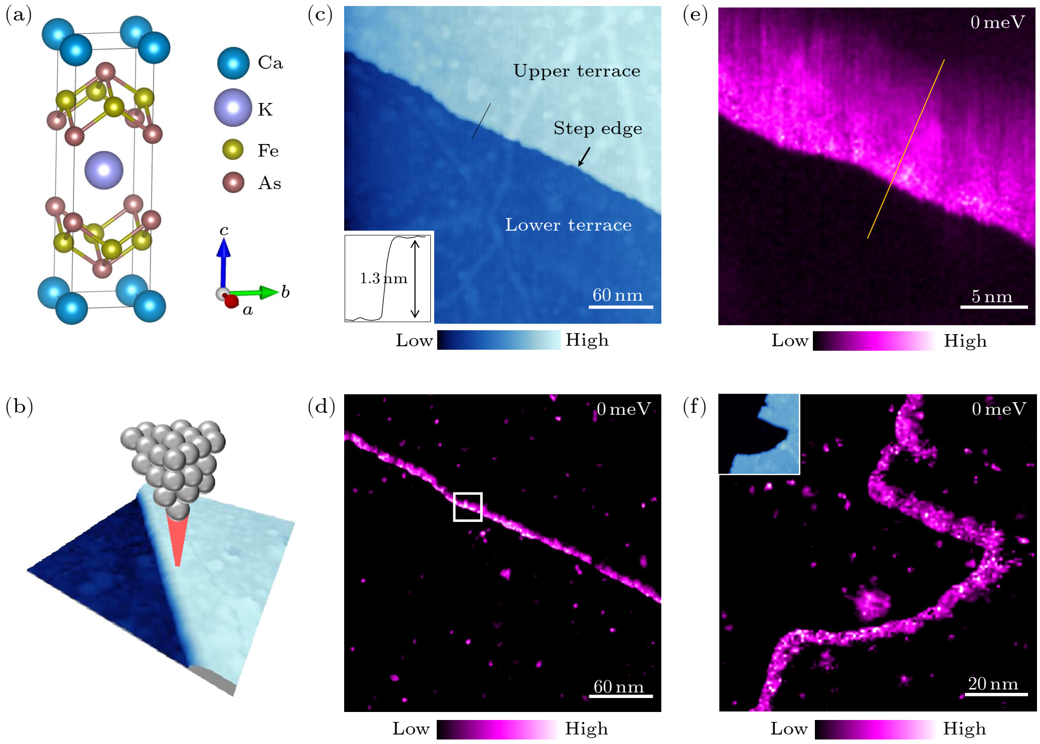

Fig. 1. Crystal structure and step edge state of $CaKFe_4As_4$. (a) Crystal structure model of $CaKFe_4As_4$. (b) Schematic of STM experimental configuration. (c) An STM topography image of cleaved $CaKFe_4As_4$ surface (size: 300 nm × 300 nm; setpoint: $V_s = -25$ mV, $I_t = 20$ pA). A distinct edge is visible between the upper terrace and the lower terrace. Inset: the line profile of the step, indicating a height of 1.3 nm. (d) Zero-energy differential conductance map of (c), showing a continuous step edge state. (e) Zoom-in 25 nm × 25 nm map from the step shown in (d) at 0 meV. (f) Zero-energy differential conductance map of the step edge which has a kink, showing that the pronounced step edge state is continuous. Inset: the corresponding STM topography [setpoint in (d)–(f): $V_s = -5$ mV, $I_t = 200$ pA]. Here, some bright spots away from step are attributed to impurities and disorders, which are commonly found on cleaved $CaKFe_4As_4$ surface.[21]

A direct comparison of the dI/dV spectra at the lower terrace (blue curve), the step (red curve) and the upper terrace (green curve) of the line cut [Fig. 2(a) and 2(b)] highlights the difference of the DOS at and away from the step edge. Away from the step, the spectra possess all the features of a clean and hard U-shaped superconducting gap, with the two coherence peaks locating at about ± 5 meV.[7] Close to the step, the coherence peaks are strongly suppressed and the gap is filled with non-zero DOS. More remarkably, a zero-bias peak (ZBP) and a series of discrete peaks emerge inside the gap. The waterfall plot [Fig. 2(c)] and the intensity map [Fig. 2(d)] show the spatial evolvement of these edge states. The ZBP has a decay length of ~ 8 nm, consistent with the decay of the step edge state [the orange curve in Fig. 2(e)]. The full width at half maximum of the ZBP is about 0.37 meV, which is close to the energy resolution of STM (0.31 meV).

More intriguingly, the ZBPs and other discrete peaks appear to be bundled in patches along the edge, as three batches of ZBP regions can be well resolved within 12 nm [Figs. 3(a) and 3(b)]. We note that this patch-type distribution of the ZBP regions is reproducible on different steps, though the distribution of the batches varies [see Fig. S7 in the Supplementary Material]. Away from the step edge, only the full superconducting gap is observed [Fig. S8]. We also find that the discrete peaks locate at energies of -1.72, -1.03, -0.64, 0, $+0.67$, and $+1.25$ meV, showing a nearly integer-quantized sequence with an energy spacing of ~ 0.6 meV [see Fig. S2(a)]. These peaks show no spatial dispersion along the perpendicular line cut, which is reminiscent of the behavior of the Caroli–de Gennes–Matricon bound states (CBS) inside the topological vortices[6,7,15] of the same material under the quantum limit [Fig. S2(b)], albeit that the energy spacings of the discrete peaks are smaller than those inside the vortex cores and the energy gap is smaller at the edge [Fig. 3(c)]. This is completely unexpected since there is no magnetic field applied.

We find evidence for the reduction of the superconducting gap near the edge, as described in the following. Away from the step edge, a well-defined peak around $-18.4\,\mathrm{mV}$ is presented in the dI/dV spectra, corresponding to the van Hove singularity (vHS).[22] It gradually shifts to about $-10\,\mathrm{mV}$ at the step edge [Fig. 3(d)], indicating hole doping effect. This hole doping effect stays at the same level within $\sim 8\,\mathrm{nm}$ from step edge, whereas it starts to decrease from ~ 8 to $\sim 10\,\mathrm{nm}$ [Fig. S9]. However, the discrete peaks only exist within $\sim 5\,\mathrm{nm}$ from the step edge [Fig. 2(d)] before fading out, giving rise to spatially unchanged energy spacing $\varDelta^2/E_{\rm F}$. It is known that hole doping over 0.4 in its sibling $\mathrm{Ba}_{1-x}\mathrm{K}_x\mathrm{Fe}_2\mathrm{As}_2$ would reduce the superconducting transition temperature and the superconducting gap. We also find that the magnetic field can induce vortices along the step edge [Fig. S3], supporting that the edge remains superconducting. The size of the vortex at the edge is larger than that away from the edge, indicating a smaller superconducting gap at the edge.

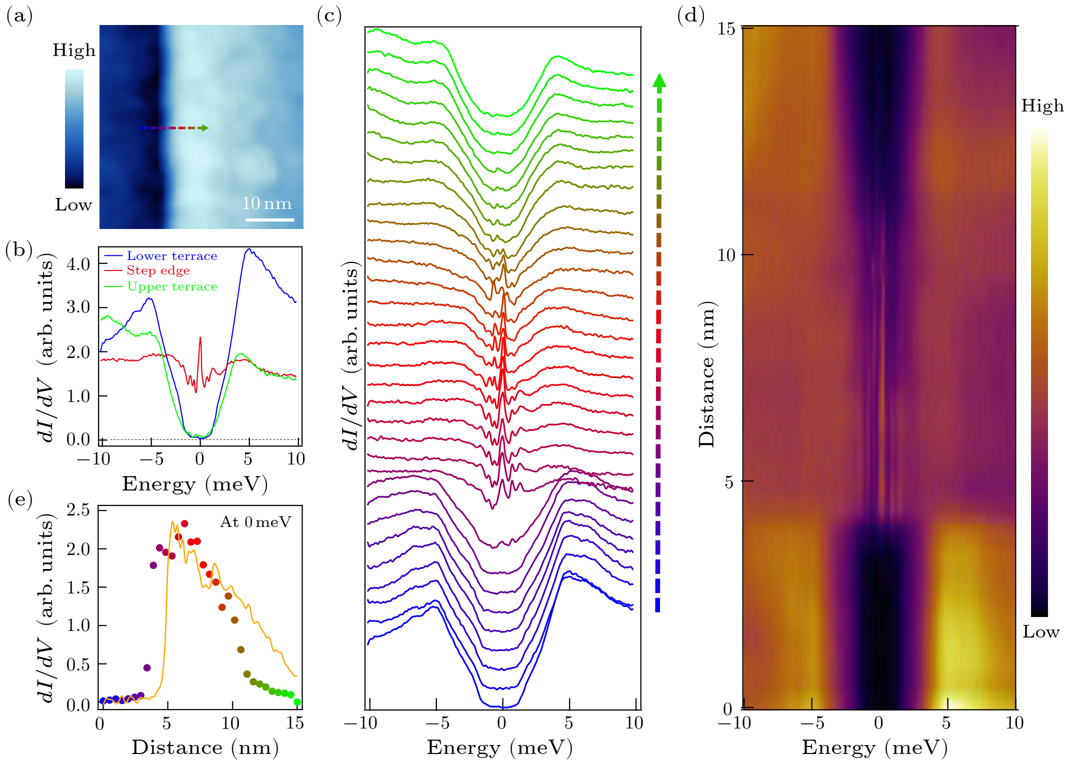

Fig. 2. The dI/dV spectra across 1-u.c. step edge. (a) A typical STM image of the 1-u.c. step edge, showing a clean and straight step. (b) Comparison of dI/dV spectra at the lower terrace (blue line), the step edge (red line), and the upper terrace (green line). The superconducting coherence peak is suppressed while the zero-bias peak (ZBP) as well as other discrete peaks emerge at the step edge. (c) A water-fall plot of the dI/dV spectra line cut measured across the step edge as marked in (a) showing that the ZBP and other non-zero discrete peaks have no energy dispersion over the line cut. (d) A line cut intensity map of the dI/dV spectra of (c). Setpoint in (b)–(d): $V_{\rm s} = -10\,\mathrm{mV}$, $I_{\rm t} = 500\,\mathrm{pA}$. (e) Colored dots: spatial dependence of zero-bias intensity of each dI/dV spectrum shown in (c). The extension length of ZBP is about 8 nm. Orange curve: zero-energy intensity line profile extracted from the line marked in Fig. 1(e).

We extract the value of peaks' energy positions $E_{\rm L}$ as well as the first level energy spacing ΔE, and plot the ratio $E_{\rm L}/\Delta E$ versus energy level n [see Fig. 3(e)]. The experimental result agrees well with integer expectation where $E_{\rm L}/\Delta E = n$ [gray line in Fig. 3(e)]. To calculate the ratios $\varDelta^2/(E_{\rm F}\cdot\Delta E)$ for both bulk and step edge states, we extract the superconducting gap $\varDelta_{\rm edge}$ of the edge states and the discrete peak spacing $\Delta E_{\rm dis}$ in fifteen cases. The Fermi energy $E_{\rm F}^{\rm edge}$ near the step is estimated to be $\sim 30\,\mathrm{meV}$ given the measured Dirac point of the topological surface state[7] and the observed vHS shift. The values of $\varDelta_{\rm S}$ and $\Delta E_{\rm CBS}$ are adopted from our previous work.[7] The values of $\varDelta^2/(E_{\rm F}\cdot\Delta E)$ for both the bulk and the step edge states are the same within error bars [Fig. 3(f)]. It again suggests that the ZBP and discrete peaks at the step edge may have the similar physical origin with the MZM and discrete CBSs in the topological vortices.

Now we discuss possible origins of the edge states. It is known that local topological trivial defects may induce states within the superconducting gap.[23] Some sign-changing superconductors such as cuprates can also have the Andreev bound states along the step edge with specific orientations.[24] However, the edge state of $CaKFe_4As_4$ is quite exotic and could not be explained by the mechanisms mentioned above. Firstly, the ubiquitous and continuous edge state appears at arbitrarily oriented integer-unit-cell steps in $CaKFe_4As_4$ (see Fig. S5 in the Supplementary Material), and displays a homogeneous decay length of ~ 10 nm into the upper terrace at any location of the step edge, which excludes the possibility of local effect from defects or the Andreev bound states.[24] Secondly, there are not only a sharp ZBP but also other non-zero-energy peaks, which is akin to the discrete bound states inside $CaKFe_4As_4$ vortex cores.[7] Thirdly, in previous reports of other 122-type FeSCs without topological surface state, e.g., $Ba_{0.6}K_{0.4}Fe_2As_2$[25] and $RbFe_2As_2$,[26] no similar edge state is observed, indicating that the robust edge state in $CaKFe_4As_4$ has a topologically non-trivial nature. Therefore, we speculate that the observed edge state has topologically non-trivial origin.

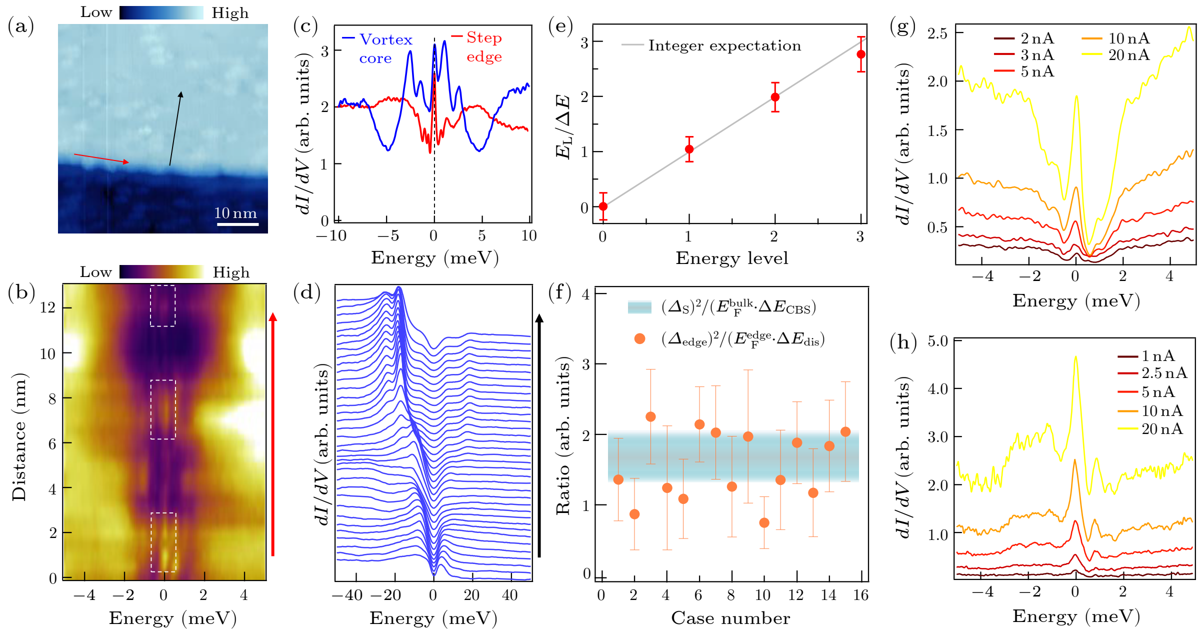

Fig. 3. Spatial dependence of in-gap bound states and van Hove singularity. (a) Topography of a step where scattered clusters distributed on the surface. (b) A line cut intensity map of the dI/dV spectra along the step edge, highlighting the three ZBP patches by the white dashed rectangles. (c) Comparison of dI/dV spectra at the vortex core (blue curve) and the step edge (red curve). The dashed line indicates the zero energy. (d) Waterfall plot of the large range dI/dV spectra along the black line in (a), showing the shift of energy position of van Hove singularity. (e) Plot of $E_{\rm L}/\Delta E$ versus energy level n. The gray line is the integer expectation which is calculated using $E_{\rm L}/\Delta E = n$. (f) Statistics of the ratio $\Delta^2/(E_{\rm F}\cdot\Delta E)$ for vortex and step edge. For vortex, Δ is the topological gap $\Delta_{\rm S} = 5.8$ meV, $E_{\rm F}$ is the topological band Fermi energy $E_{\rm F}^{\rm bulk} = 21$ meV, ΔE is the CBS spacing from our previous work $\Delta E_{\rm CBS} = 0.8$–1.2 meV. For step edge, Δ is the superconducting gap on step edge $\Delta_{\rm edge}$, $E_{\rm F}$ is the Fermi energy on step edge $E_{\rm F}^{\rm edge} \approx 30$ meV, ΔE is the discrete peak spacing on step edge $\Delta E_{\rm dis}$. (g)–(h) Two examples of the tunneling current dependent dI/dV spectra. $V_{\rm s} = -5$ mV, $I_{\rm t}$ is labeled in figures for each curve. The zero-bias peak remains robust and has no split behavior when tip-sample distance is decreased.

Another trivial origin of the ZBP is the Yu–Shiba–Rusinov (YSR) state, which can be distinguished by using superconducting or spin-polarized tip state.[27] However, these experiments seem to be extremely difficult on the cleaved surfaces of $CaKFe_4As_4$, because the surfaces are covered by unstable Ca or K atoms/clusters.[28] We found that these atoms/clusters could be picked up easily by tip during scanning process, which could destroy the superconducting or spin-polarized state of the tip. To exclude the YSR state, we decrease the tip-sample distance while measuring the dI/dV spectra with ZBP. Two examples are shown in Figs. 3(g)–3(h). It can be found that the ZBP does not split even at a high tunneling current of ~ 20 nA, suggesting the absence of YSR state which is expected to split at such decreased tip-sample distance.[29] We also found that, once the tunneling current exceeds ~ 30 nA, the tunneling junction at the step edge would become unstable, leading to the tip crashing into the sample. As a result, we did not observe the plateau feature of ZBP. This phenomenon provides evidence to exclude the possibility of the trivial YSR state.

Here, we propose that the edge state in $CaKFe_4As_4$ is the result of cooperation between the topological surface states and the possible time-reversal symmetry breaking (TRSB) pairings with different symmetries.[30,31] In the 122-family FeSCs, the gap functions on two Fermi pockets couple in the anti-phase way due to repulsive interactions.[1–4] This feature could lead to frustration due to the existence of three Fermi pockets including two hole ones and an electron one.[31] When hole doping is relatively small, the gap function is likely a time-reversal invariant s-wave, s_{++-} representing the gap function configuration (Δ_{h1}, Δ_{h2}, $-\Delta_e$) where the former two are of two hole-bands. With increasing hole doping, Δ_e is weakened, then the anti-phase couplings lead to the configuration (Δ_{h1}, $\Delta_{h2}e^{i\varphi_h}$, $\Delta_e e^{i\varphi_e}$). Time-reversal symmetry is broken at $\varphi_{h,e} \neq 0, \pi$. For simplicity, this pairing configuration is hereafter denoted as $s+is$ in agreement with the convention in literature [Fig. 4(a)]. Recent experimental studies based on muon-spin-rotation (μSR) measurements in heavily hole-doped $Ba_{1-x}K_xFe_2As_2$ (where $x = 0.77$–0.8)[32,33] and the temperature-dependent fractional quantum vortex in the same material[34] provide strong evidence of an $s+is$ superconducting pairing order parameter which breaks time-reversal symmetry. Also, time-resolved optical reflectivity experiments support the existence of time-reversal symmetry breaking state in $CaKFe_4As_4$.[35] The shift of the vHS peak [Fig. 3(d)] suggests that increasing hole doping level may drive the step edge into a similar $s+is$ state with a small superconducting gap. Previous theoretical work suggests that an $s_\pm$ superconductor has a tendency to develop the $s+is$ state near the boundary,[36,37] which may widen the narrow doping range of the $s+is$ state as appeared in $Ba_{1-x}K_xFe_2As_2$ ($x = 0.77$–0.8).

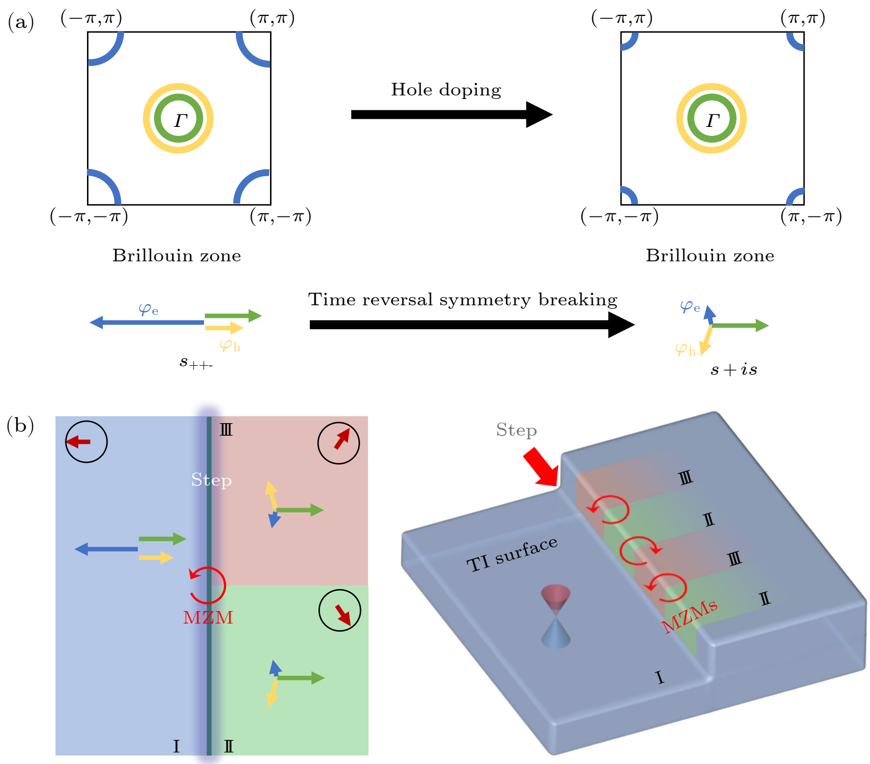

Fig. 4. Schematic of emergence of MZM at the step. (a) Gap functions and Fermi surface evolution with the increasing hole doping. The blue arrow represents the gap function on the electron pocket, and the green and yellow ones represent those on the hole pockets. At small hole doping, the gap functions are time-reversal invariant and sign changing denoted as s_{++-}. At large hole doping, frustration becomes effective, and TRSB gap functions take place. (b) Schematics of the surface near the step edge. Superconducting gap functions in the blue region are time-reversal invariant, which lie in the lower terrace and upper terrace away from the step edge. Green and red regions are on the upper terrace and near the step edge representing two domains with TRSB gap functions, which are time-reversal counterparts. The gap parameters induced in the Dirac surface states are combined effect of the multi-band gap functions in the bulk. When they in the three regions form a vortex-like defect, the MZM appears at the crossing point of the tri-junction. With further going deep inside the upper terrace, the gap parameters smoothly relax to the time-reversal invariant one without forming a vortex-like defect.

Once such TRSB superconductivity happens on the topological surface topological state in the $CaKFe_4As_4$ system,[7] the Dirac surface state will acquire a gap function by the proximity effect expressed as

$$H_{\rm surf} = v_F(k_x s_y \otimes \tau_0 - k_y s_x \otimes \tau_3) - \mu s_0 \otimes \tau_3 \\ - [{\rm Re}\Delta] s_y \otimes \tau_2 - [{\rm Im}\Delta] s_y \otimes \tau_1.$$

Here, v_F is the Fermi velocity of the Dirac state; s_j ($j = x, y, z$) represent spin operators and τ_n ($n = 1, 2, 3$) denote Pauli matrices in the Nambu channel; s_0 and τ_0 are identity matrices in the spin space and Nambu channels, respectively. $\Delta = \alpha(\Delta_{h1} + \Delta_{h2}e^{i\varphi_h} + \Delta_e e^{i\varphi_e})$, where α is dimensionless coefficient depending on the proximity effectiveness, and for simplicity it is assumed the same for all the bands. Around the step edge shown in Fig. 3(a), a tri-junction configuration illustrated in Fig. 4(a) may appear, which consists of three regions: the lower terrace with time-reversal invariant gap functions (Δ_{h1}, Δ_{h2}, $-\Delta_e$) (I), and the upper terrace with a pair of TRSB counterparts exhibiting gap function configurations (Ⅱ) ($\Delta'_{\rm h1}$, $\Delta'_{\rm h2}e^{i\varphi_{\rm h}}$, $\Delta'_{\rm e}e^{i\varphi_{\rm e}}$) and (Ⅲ) ($\Delta'_{\rm h1}$, $\Delta'_{\rm h2}e^{-i\varphi_{\rm h}}$, $\Delta'_{\rm e}e^{-i\varphi_{\rm e}}$), respectively. Without loss of generality, $\Delta_{\rm h1,2}$ are assumed to be positive, and $\Delta_{\rm e}$ is stronger than $\Delta_{\rm h1,2}$. We assume that $\Delta_{\rm h1}$ is aligned in all the three regions, such that the gap functions on the other two bands develop a non-collinear configuration. Up to an overall phase, the surface Dirac states in these regions acquire a real gap parameter Δ by the proximity effect in region (I), and complex ones Δ' Δ'^{*} in regions (Ⅱ) and (Ⅲ), respectively. An MZM will appear near the tri-junction region if the above gap parameters in the surface Dirac states in the three regions resemble a vortex-like topological defect, i.e., their phases complete a 2π winding.[38]

The presence of two regions with complex gap functions on the upper terrace alternates along the edge. While a single MZM appears at the center of a tri-junction, the repeated presence of separate MZMs along the edge is anticipated [Fig. 4(b)]. When moving away from the step edge on the upper terrace, the hole doping gradually relaxes to the bulk value. Another anti-vortex-like defect should also exist, nevertheless, the core area and the associated MZM may be smeared and not easy to observe deep inside the upper terrace. This mechanism also applies to higher step edges (Fig. S5 in the Supplementary Material). The hole-doping effect can occur at such step edges (Fig. S6), driving the system into a possible state that breaks time-reversal symmetry. Consequently, MZMs can also be observed.

In conclusion, we observe robust zero-energy modes on step of $CaKFe_4As_4$ with peculiar features. At some step locations, ZBPs and discrete peaks with equal energy spacing are observed in dI/dV spectra under zero magnetic field, akin to the MZM and integer CBSs observed in the topological vortex of the same material. Based on the vHS shift at step edge, we propose that the step edge hosts a possible time-reversal symmetry breaking state, such as $s+is$ state, and the observed ZBP can be interpreted as an MZM inside an effective vortex generated at the center of a tri-junction with different superconducting order parameters. Our discovery not only opens a new way of generating MZMs without magnetic field, but also provides deep insights for evolutions of the superconducting pairing states in FeSCs, and calls for more efforts on direct experimental probe for this possible time-reversal symmetry breaking state.

Experimental Method.

Single Crystal Growth. High-quality single crystals of $CaKFe_4As_4$ were grown by using the self-flux method. The value of $T_{\rm c}$ was determined to be 35 K from magnetization measurements.

Scanning Tunneling Microscopy/Spectroscopy. The samples used in STM/S experiments were cleaved *in situ* ($T_{\rm cleave} = 77$ K) and immediately transferred to the STM head. Chemically etched tungsten tips were calibrated on Au(111) surface before use. STM/S measurements were performed in two ultra-high vacuum (1×10^{-11} mbar) LT-STM systems, STM#1 (base temperature 30 mK) and STM#2 (base temperature 400 mK). The differential conductance (dI/dV) spectra and map were obtained by a standard lock-in amplifier at a frequency of 973.0 Hz, with the modulation voltage $V_{\rm mod} = 0.05$ mV for STM#1 and $V_{\rm mod} = 0.10$ mV for STM#2.

Acknowledgment. We thank Vadim Grinenko and Kun Jiang for help discussions. This work was supported by the National Key Research and Development Program of China (Grant No. 2019YFA0308500), the National Natural Science Foundation of China (Grant Nos. 62488201, 52072401, 11888101, 12234016, and 12174317), the Chinese Academy of Sciences (Grant No. YSBR-003), the Innovation Program of Quantum Science and Technology (Grant No. 2021ZD0302700), the New Cornerstone Science Foundation, the China Postdoctoral Science Foundation (Grant No. 2022M723111), and the Fellowship of China National Postdoctoral Program for Innovative Talents (Grant No. BX20230358).

References

[1] Paglione J and Greene R L 2010 *Nat. Phys.* **6** 645
[2] Stewart G R 2011 *Rev. Mod. Phys.* **83** 1589
[3] Si Q, Yu R, and Abrahams E 2016 *Nat. Rev. Mater.* **1** 16017
[4] Fernandes R M, Coldea A I, Ding H, Fisher I R, Hirschfeld P J, and Kotliar G 2022 *Nature* **601** 35
[5] Zhang P, Yaji K, Hashimoto T, Ota Y, Kondo T, Okazaki K, Wang Z J, Wen J S, Gu G D, Ding H, and Shin S 2018 *Science* **360** 182
[6] Liu Q, Chen C, Zhang T, Peng R, Yan Y J, Wen C H P, Lou X, Huang Y L, Tian J P, Dong X L, Wang G W, Bao W C, Wang Q H, Yin Z P, Zhao Z X, and Feng D L 2018 *Phys. Rev. X* **8** 041056
[7] Liu W, Cao L, Zhu S, Kong L, Wang G, Papaj M, Zhang P, Liu Y B, Chen H, Li G, Yang F, Kondo T, Du S, Cao G H, Shin S, Fu L, Yin Z, Gao H J, and Ding H 2020 *Nat. Commun.* **11** 5688
[8] Zhang P, Wang Z, Wu X, Yaji K, Ishida Y, Kohama Y, Dai G, Sun Y, Bareille C, Kuroda K, Kondo T, Okazaki K, Kindo K, Wang X, Jin C, Hu J, Thomale R, Sumida K, Wu S, Miyamoto K, Okuda T, Ding H, Gu G D, Tamegai T, Kawakami T, Sato M, and Shin S 2019 *Nat. Phys.* **15** 41
[9] Kong L, Cao L, Zhu S, Papaj M, Dai G, Li G, Fan P, Liu W, Yang F, Wang X, Du S, Jin C, Fu L, Gao H J, and Ding H 2021 *Nat. Commun.* **12** 4146
[10] Cao L, Liu W, Li G, Dai G, Zheng Q, Wang Y, Jiang K, Zhu S, Huang L, Kong L, Yang F, Wang X, Zhou W, Lin X, Hu J, Jin C, Ding H, and Gao H J 2021 *Nat. Commun.* **12** 6312
[11] Li M, Li G, Cao L, Zhou X, Wang X, Jin C, Chiu C K, Pennycook S J, Wang Z, and Gao H J 2022 *Nature* **606** 890
[12] Liu W, Hu Q, Wang X, Zhong Y, Yang F, Kong L, Cao L, Li G, Peng Y, Okazaki K, Kondo T, Jin C, Xu J, Gao H J, and Ding H 2022 *Quantum Front.* **1** 20
[13] Kallin C and Berlinsky J 2016 *Rep. Prog. Phys.* **79** 054502
[14] Wang D F, Kong L Y, Fan P, Chen H, Zhu S Y, Liu W Y, Cao L, Sun Y J, Du S X, Schneeloch J, Zhong R D, Gu G D, Fu L, Ding H, and Gao H J 2018 *Science* **362** 333
[15] Kong L, Zhu S, Papaj M, Chen H, Cao L, Isobe H, Xing Y, Liu W, Wang D, Fan P, Sun Y, Du S, Schneeloch J, Zhong R, Gu G, Fu L, Gao H J, and Ding H 2019 *Nat. Phys.* **15** 1181
[16] Machida T, Sun Y, Pyon S, Takeda S, Kohsaka Y, Hanaguri T, Sasagawa T, and Tamegai T 2019 *Nat. Mater.* **18** 811

[17] Zhu S Y, Kong L Y, Cao L, Chen H, Papaj M, Du S X, Xing Y Q, Liu W Y, Wang D F, Shen C M, Yang F Z, Schneeloch J, Zhong R D, Gu G D, Fu L, Zhang Y Y, Ding H, and Gao H J 2020 *Science* **367** 189
[18] Wang Z Y, Rodriguez J O, Jiao L, Howard S, Graham M, Gu G D, Hughes T L, Morr D K, and Madhavan V 2020 *Science* **367** 104
[19] Iyo A, Kawashima K, Kinjo T, Nishio T, Ishida S, Fujihisa H, Gotoh Y, Kihou K, Eisaki H, and Yoshida Y 2016 *J. Am. Chem. Soc.* **138** 3410
[20] Chen C, Jiang K, Zhang Y, Liu C F, Liu Y, Wang Z Q, and Wang J 2020 *Nat. Phys.* **16** 536
[21] Fente A, Meier W R, Kong T, Kogan V G, Bud'ko S L, Canfield P C, Guillamón I, and Suderow H 2018 *Phys. Rev. B* **97** 134501
[22] Fang D, Shi X, Du Z, Richard P, Yang H, Wu X X, Zhang P, Qian T, Ding X, Wang Z, Kim T K, Hoesch M, Wang A, Chen X, Hu J, Ding H, and Wen H H 2015 *Phys. Rev. B* **92** 144513
[23] Hanaguri T, Niitaka S, Kuroki K, and Takagi H 2010 *Science* **328** 474
[24] Misra S, Oh S, Hornbaker D J, DiLuccio T, Eckstein J N, and Yazdani A 2002 *Phys. Rev. B* **66** 100510
[25] Shan L, Wang Y L, Shen B, Zeng B, Huang Y, Li A, Wang D, Yang H, Ren C, Wang Q H, Pan S H, and Wen H H 2011 *Nat. Phys.* **7** 325
[26] Liu X, Tao R, Ren M, Chen W, Yao Q, Wolf T, Yan Y, Zhang T, and Feng D 2019 *Nat. Commun.* **10** 1039
[27] Jäck B, Xie Y, and Yazdani A 2021 *Nat. Rev. Phys.* **3** 541
[28] Cao L, Song Y, Liu Y B, Zheng Q, Han G, Liu W, Li M, Chen H, Xing Y, Cao G H, Ding H, Lin X, Du S, Zhang Y Y, Li G, Wang Z, and Gao H J 2021 *Nano Res.* **14** 3921
[29] Farinacci L, Ahmadi G, Reecht G, Ruby M, Bogdanoff N, Peters O, Heinrich B W, von Oppen F, and Franke K J 2018 *Phys. Rev. Lett.* **121** 196803
[30] Lee W C, Zhang S C, and Wu C 2009 *Phys. Rev. Lett.* **102** 217002
[31] Maiti S and Chubukov A V 2013 *Phys. Rev. B* **87** 144511
[32] Grinenko V, Materne P, Sarkar R, Luetkens H, Kihou K, Lee C H, Akhmadaliev S, Efremov D V, Drechsler S L, and Klauss H H 2017 *Phys. Rev. B* **95** 214511
[33] Grinenko V, Sarkar R, Kihou K, Lee C H, Morozov I, Aswartham S, Büchner B, Chekhonin P, Skrotzki W, Nenkov K, Hühne R, Nielsch K, Drechsler S L, Vadimov V L, Silaev M A, Volkov P A, Eremin I, Luetkens H, and Klauss H H 2020 *Nat. Phys.* **16** 789
[34] Iguchi Y, Shi R A, Kihou K, Lee C H, Barkman M, Benfenati A L, Grinenko V, Babaev E, and Moler K A 2023 *Science* **380** 1244
[35] Zhao S Z, Song H Y, Hu L L, Xie T, Liu C, Luo H Q, Jiang C Y, Zhang X, Nie X C, Meng J Q, Duan Y X, Liu S B, Xie H Y, and Liu H Y 2020 *Phys. Rev. B* **102** 144519
[36] Bobkov A M and Bobkova I V 2011 *Phys. Rev. B* **84** 134527
[37] Benfenati A and Babaev E 2022 *Phys. Rev. B* **105** 134518
[38] Fu L and Kane C L 2008 *Phys. Rev. Lett.* **100** 096407

Supplementary Material for

Observation of zero-energy modes with possible time-reversal symmetry breaking on step edge of $CaKFe_4As_4$

Lu Cao(曹路)[1,2,†], Geng Li(李更)[1,2,3,†], Wenyao Liu(刘文尧)[1,2,3,†], Ya-Bin Liu(刘亚彬)[4], Hui Chen(陈辉)[1,2], Yuqing Xing(邢宇庆)[1,2], Lingyuan Kong(孔令元)[1,2], Fazhi Yang(杨发枝)[1,2,3], Quanxin Hu(胡全欣)[1,2,3], Meng Li(李萌)[1,2], Xingtai Zhou(周兴泰)[1,2], Zichao Chen(陈子超)[1,2], Chenhang Ke(柯晨航)[5], Lunhui Hu(胡仑辉)[4], Guang-Han Cao(曹光旱)[4], Congjun Wu(吴从军)[5,6,7,8], Hong Ding(丁洪)[9,1,3*], and Hong-Jun Gao(高鸿钧)[1,2,3*]

[1] Institute of Physics, Chinese Academy of Sciences, Beijing 100190, China

[2] School of Physical Sciences, University of Chinese Academy of Sciences, Beijing 100049, China

[3] Hefei National Laboratory, Hefei 230088, China

[4] Department of Physics, Zhejiang University, Hangzhou 310027, China

[5] New Cornerstone Science Laboratory, Department of Physics, School of Science, Westlake University, 310024, Hangzhou, China

[6] Institute for Theoretical Sciences, Westlake University, 310024, Hangzhou, China

[7] Key Laboratory for Quantum Materials of Zhejiang Province, School of Science, Westlake University, 310024, Hangzhou, China

[8] Institute of Natural Sciences, Westlake Institute for Advanced Study, 310024, Hangzhou, China

[9] Tsung-Dao Lee Institute, and New Cornerstone Science Laboratory, Shanghai Jiao Tong University, Shanghai, 201210, China

#These authors contributed equally to this work

*Correspondence to: hjgao@iphy.ac.cn; dingh@sjtu.edu.cn

d*I*/d*V* map of step at different energy:

The d*I*/d*V* map at low energy (Figure S1(a)-(c)) show the edge state clearly. At slight high energy (Figure S1(d)), the edge state become obscure because of the increase of non-zero intensity away from the step edge.

Multiple-peak fitting for step edge state and topological vortex core:

The multiple-peak fittings for step edge states and topological vortex core are displayed in Figure S2(a) and 2(b), respectively. The integer energy level spacings both in step edge state and topological vortex core are well-resolved.

Vortex size at step edge:

From the ZEDC map under magnetic field, we find the vortex located at the step edge has a larger size, namely the coherence length, compared to that away from step edge (Figure S3).

ZEDC maps of step edge states under different magnetic fields:

By varying the magnitudes and orientations of magnetic fields, we find the step edge states remain robust no matter under the out-of-plane or in-plane magnetic fields (Figure S4).

Reproducible result on a 2-UC step edge:

Besides the 1-UC step, the non-zero intensity in superconducting gap and ZBP are also observed on the 2-UC step edge (Figure S5), whose features are similar to that at 1-UC step.

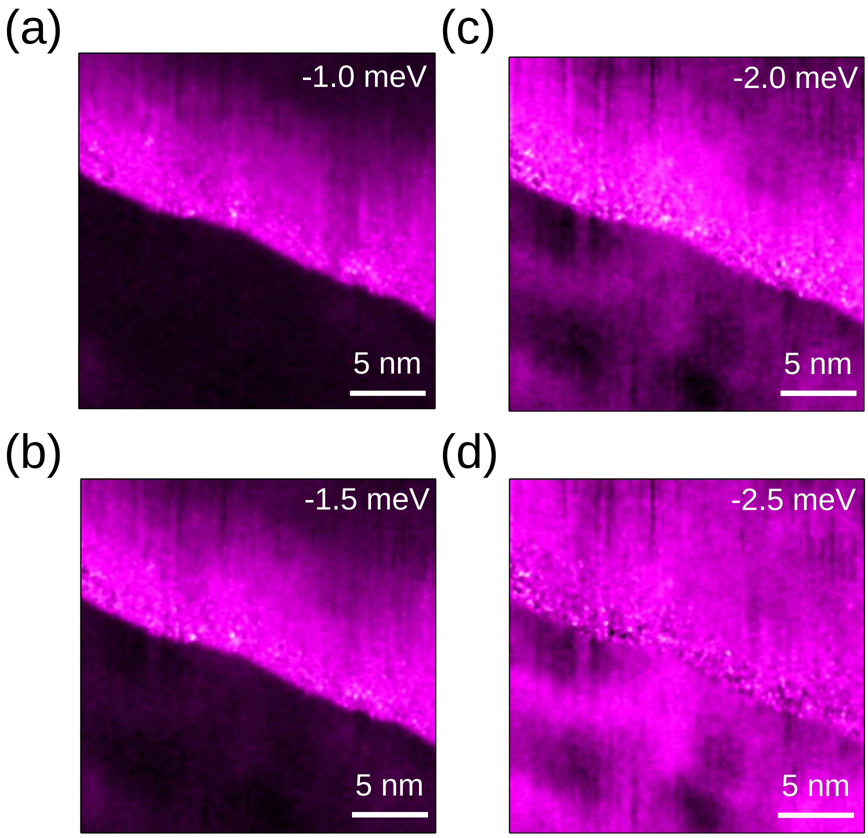

Figure S1. dI/dV map of step at different energy. (a)-(d), The zoom-in 25 nm × 25 nm dI/dV map from the step in Fig. 1(d) at −1.0, −1.5, −2.0 and −2.5 meV, respectively.

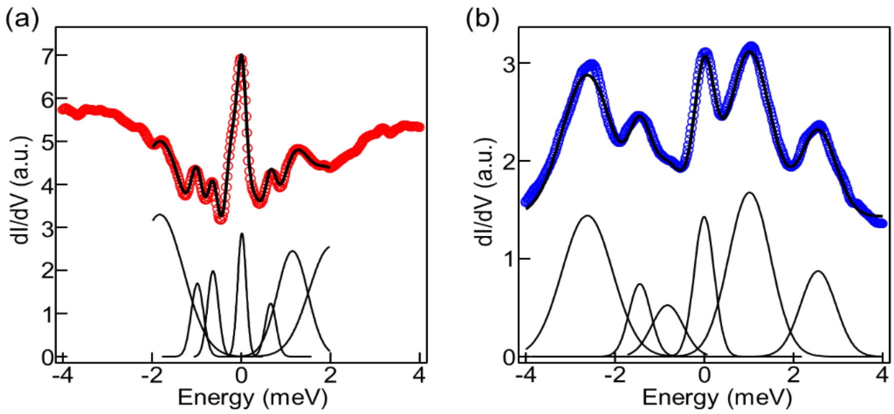

Figure S2. Fitting of peaks around zero-energy. (a), The multiple-peak fitting of ZBP and discrete peaks around zero-energy for edge state. (b), The multiple-peak fitting of MZM and CBSs around zero-energy for topological vortex. Red or blue circles are experimental data. Black curve with multiple-peak are the fitting results. Individual peaks indicate the energy locations of ZBP and non-zero discrete peaks (a), MZM and CBSs (b).

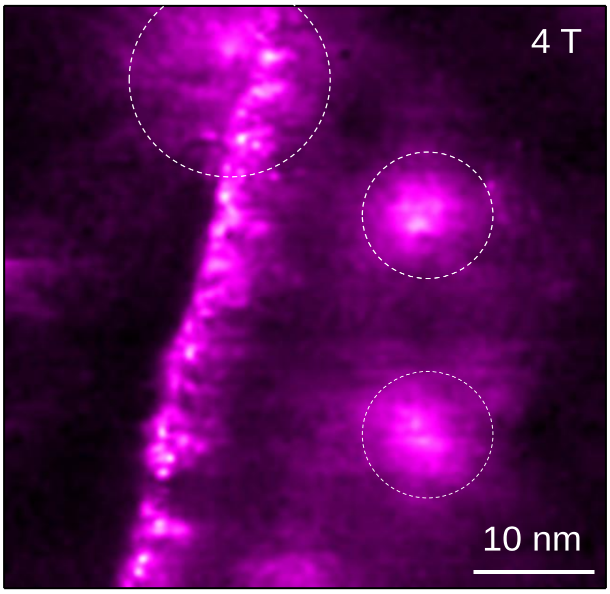

Figure S3. Emergence of larger vortices at the step edges, suggesting the superconducting nature of the edge channel as well as the larger coherence length at step edges.

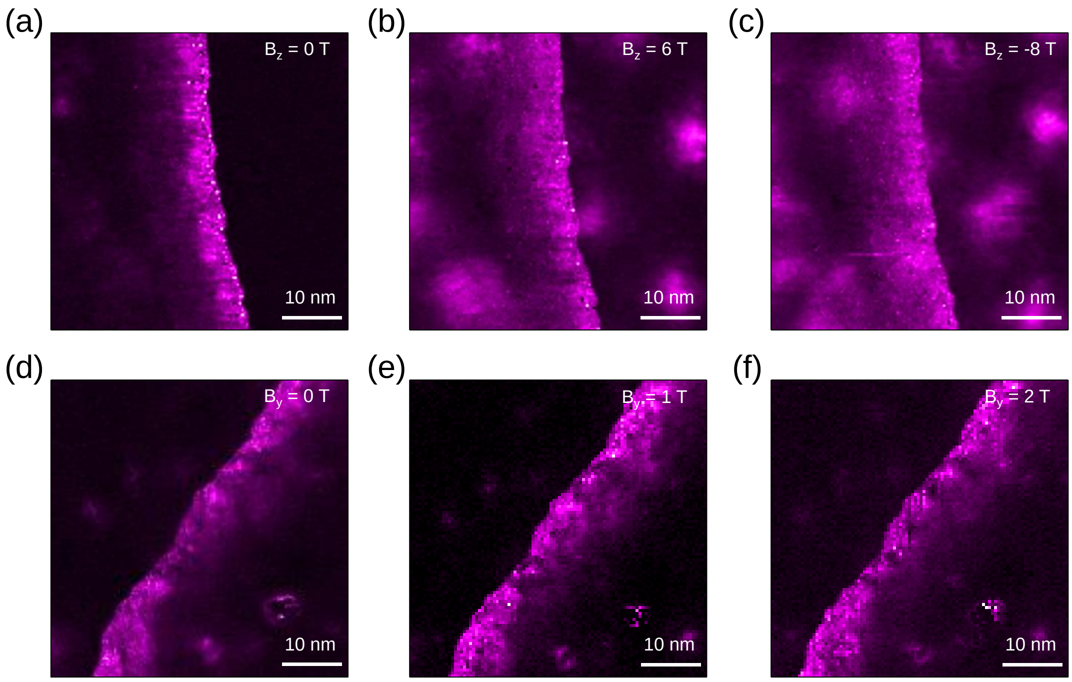

Figure S4. Magnetic field dependence of step edge state. (a)-(c), The ZEDC maps of step edge state under $B_z = 0, 6, -8$ T, respectively. (d)-(f), The ZEDC maps of step edge state under $B_y = 0, 1, 2$ T, respectively.

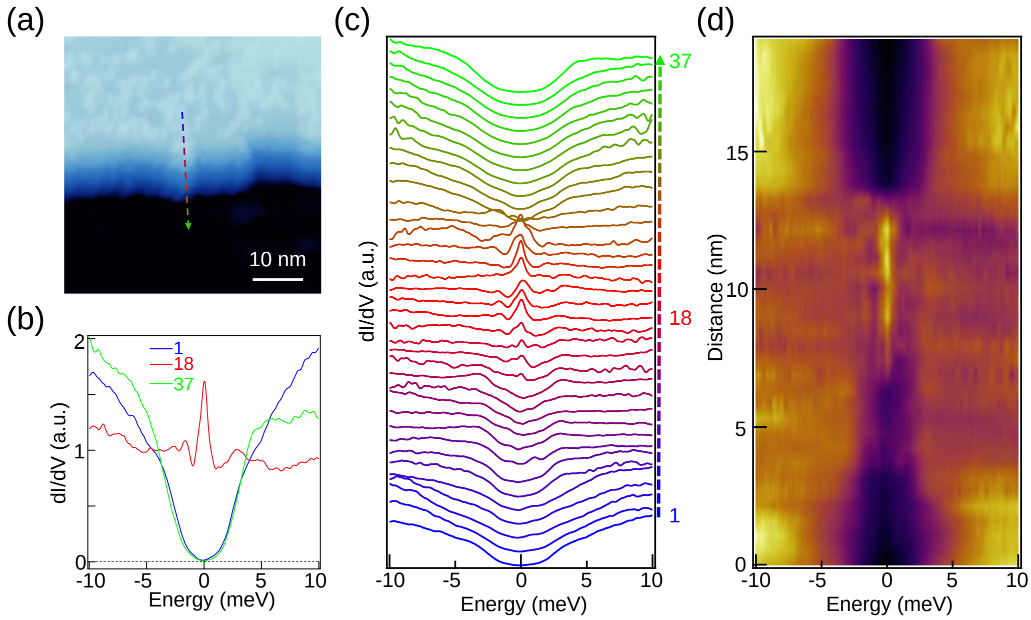

Figure S5. ZBP on 2-UC step edge. (a), the STM topography of a 2-UC height step edge. (b), The comparison of d*I*/d*V* spectra at the lower terrace (green line), the step edge (red line) and the upper terrace (blue line). (c), A water-fall plot of the d*I*/d*V* spectra line-cut measured across the 2-UC step edge as marked by the dashed arrow in (a). (d), A line-cut intensity map of the d*I*/d*V* spectra of (c). The d*I*/d*V* spectra results show the robust edge state as well as the ZBP, which are similar to that on the 1-UC step edge.

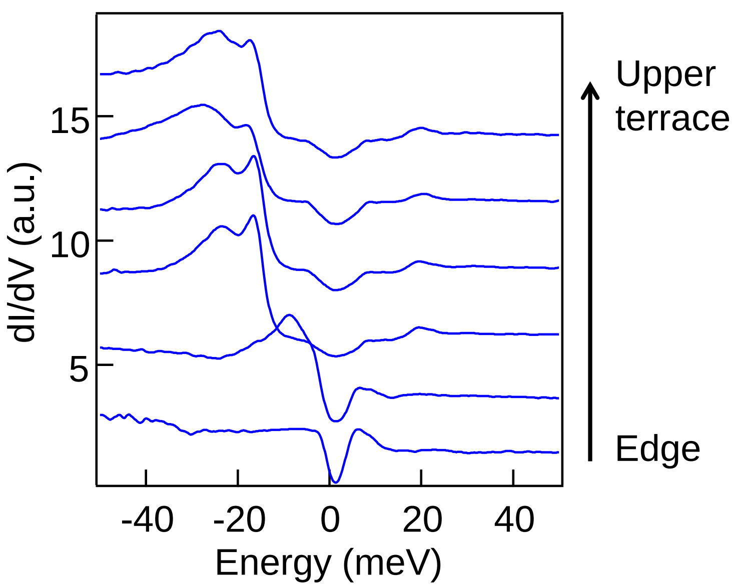

Figure S6. Waterfall-plot of the large range d*I*/d*V* spectra from the edge of a 2-UC step to the upper terrace, illustrating the doping effect at the edge.

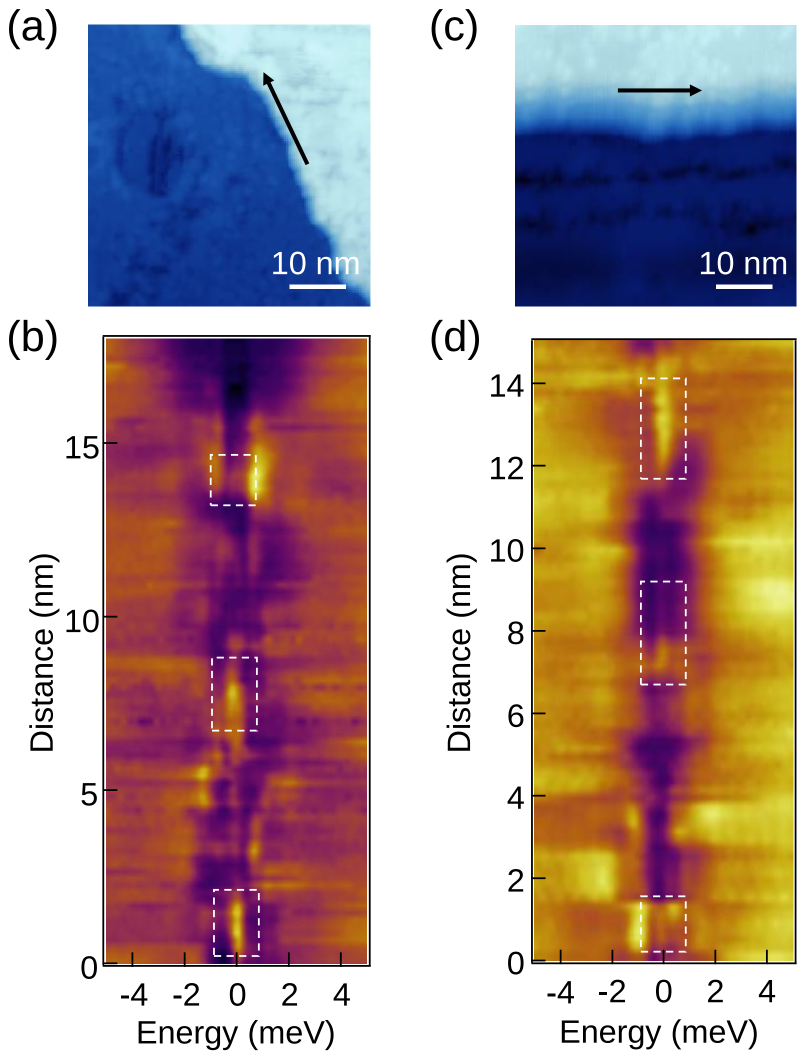

Figure S7. Reproduced results of the patch-like ZBP distribution along the step edges. (a) The topography image of a step edge. (b) Intensity map of the d*I*/d*V* spectra along the black arrow in (a). White dashed rectangles highlight the three ZBP patches. (c) and (d) Same as (a) and (b), but on a different step edge.

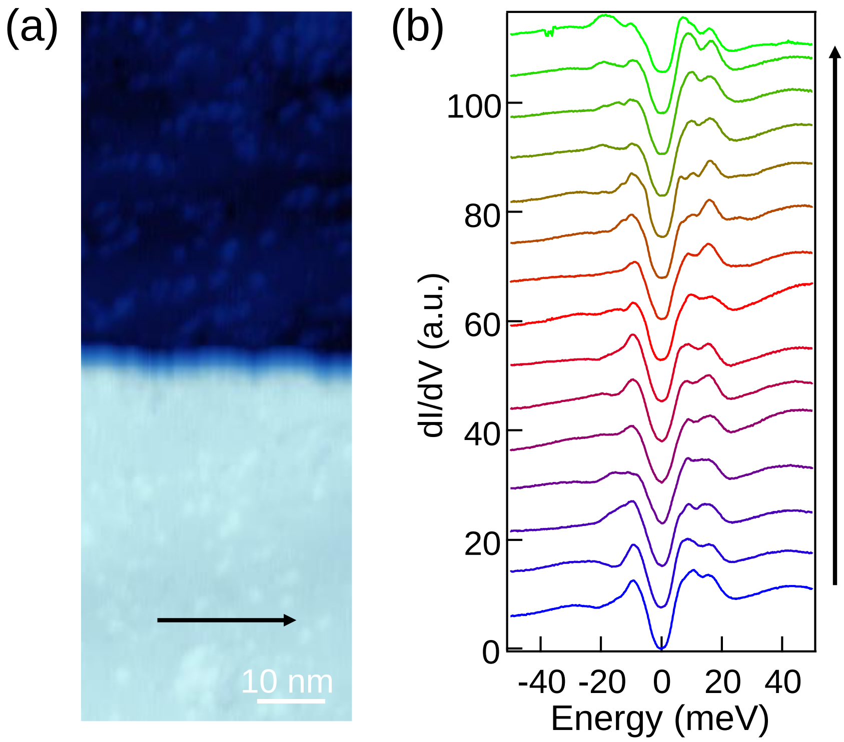

Figure S8. dI/dV spectra linecut parallel to step edge on the plateau. (a) The topography image shows a step edge. (b) The dI/dV spectra linecut along the black arrowed line as marked in (a). No zero-bias conductance peak observed.

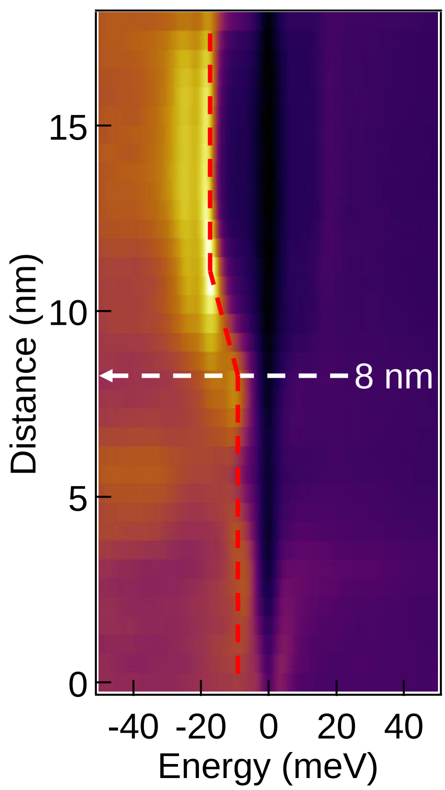

Figure S9. Intensity map plot of data in Fig. 3(d). The red dashed line marks the energy position of VHS.